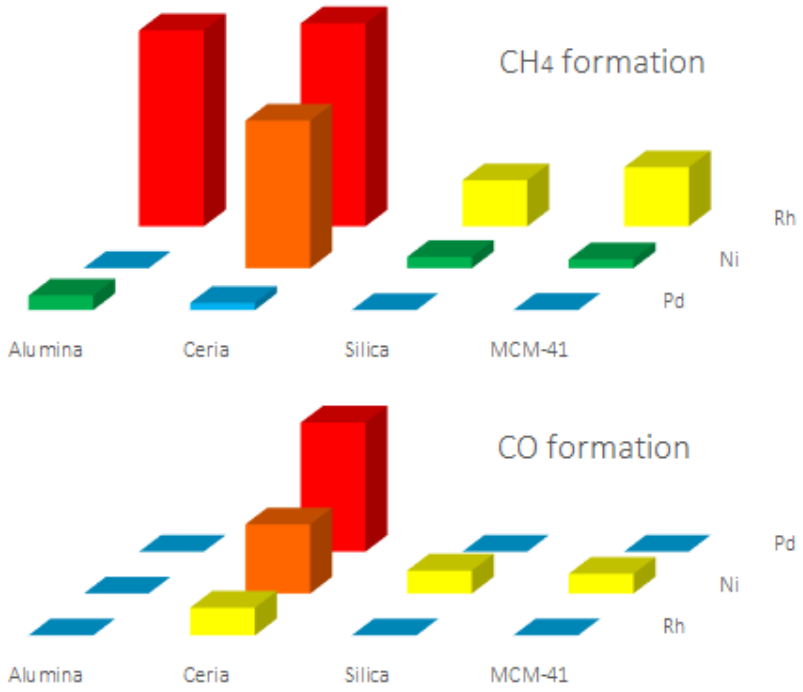
CHALMERS
UNIVERSITY OF TECHNOLOGY



Catalytic reduction of carbon dioxide for production of green fuels

Master's thesis in Materials Chemistry and Nanotechnology

Peter Velin

Department of Chemistry and Chemical Engineering
CHALMERS UNIVERSITY OF TECHNOLOGY
Gothenburg, Sweden 2015

Master's thesis 2015:June

Catalytic reduction of carbon dioxide for production of green fuels

Peter Velin



Department of Chemistry and Chemical Engineering
The Competence Centre for Catalysis
Chalmers University of Technology
Gothenburg, Sweden 2015

Catalytic reduction of carbon dioxide for production of green fuels
Peter Velin

© PETER VELIN, 2015.

Supervisors: Emma Adams, Natalia Martin
Examiner: Per-Anders Carlsson

Master's Thesis 2015:June
Department of Chemistry and Chemical Engineering
The Competence Centre for Catalysis
Chalmers University of Technology
SE-412 96 Gothenburg
Telephone +46 (0)31 772 29 7

Typeset in LaTeX
Gothenburg, Sweden 2015

Catalytic reduction of carbon dioxide for production of green fuels
Peter Velin
Department of Chemistry and Chemical Engineering
Chalmers University of Technology

Abstract

The purpose of this thesis is to evaluate whether reduction of carbon dioxide and carbon monoxide by hydrogenation over an appropriate catalyst can be used for production of green fuels. Thirteen different catalyst formulations were prepared with palladium, nickel and rhodium as active phases supported by alumina, ceria, silica, MCM-41 and ZSM-5. All structures were confirmed to be retained after impregnation and calcination, determined by specific surface area measurements and XRD analysis. Catalytic activity measurements using a chemical flow-reactor were successfully performed at atmospheric pressure, different temperatures and specific reactant ratios.

The kinetic measurements showed an increased conversion of carbon dioxide to methane and carbon monoxide at elevated temperature, with varying selectivity primarily depending on active phase. Generally, an active phase of rhodium and palladium favored the formation of methane and carbon monoxide respectively, whereas nickel catalyzed the formation of both products. The major part of increased carbon dioxide conversion observed above 350 °C was due to carbon monoxide formation *via* the reversed water gas shift reaction, independently of catalyst. Furthermore, ceria is reported to be the most active support for hydrogenation of carbon dioxide, probably due to a participating role in carbon dioxide adsorption and a highly dispersed active phase.

Deeper evaluation of the rhodium impregnated ceria catalyst showed a maximum methane formation by carbon dioxide hydrogenation at approximately 380 °C. Above this temperature the formation declined due to increased carbon monoxide formation. A suggested explanation, strengthened by carbon monoxide experiments is an increased carbon monoxide desorption rate at elevated temperatures.

Keywords: CO_2 hydrogenation, CO_2 reduction, CO hydrogenation, CH_4 formation, methanation, atmospheric pressure

Acknowledgements

This master thesis would not have been possible without the guidance from my supervisors Emma Adams and Natalia Martin, who have helped me with catalyst preparation, characterization and catalytic investigation. I would also like to thank my examiner Per-Anders Carlsson for giving me the opportunity to write my master thesis at KCK, and for all the valuable discussions we had. Gratitude is also shown to the rest of the members at KCK and TYK for being very nice to me.

Peter Velin, Gothenburg, 2015

Contents

1 Introduction **1**
- 1.1 Background . . . 1
- 1.2 Aim . . . 2

2 Theory **3**
- 2.1 Heterogeneous catalysis . . . 3
- 2.2 Catalyst materials . . . 5
  - 2.2.1 Common supports . . . 5
  - 2.2.2 Zeolites and mesoporous materials . . . 6
  - 2.2.3 Active phase . . . 6
- 2.3 Catalytic hydrogenation . . . 7

3 Experimental section **9**
- 3.1 Experimental approach . . . 9
- 3.2 Catalyst preparation . . . 9
  - 3.2.1 Incipient wetness impregnation . . . 9
  - 3.2.2 Aqueous ion-exchange . . . 9
  - 3.2.3 Washcoating . . . 10
- 3.3 Structural characterisation . . . 10
  - 3.3.1 X-ray powder diffraction . . . 10
  - 3.3.2 Specific surface area measurement . . . 11
- 3.4 Kinetic evaluation . . . 12

4 Results **15**
- 4.1 Characterization of catalysts . . . 15
- 4.2 Catalysts performance . . . 16
  - 4.2.1 Hydrogenation of CO_2 . . . 16
  - 4.2.2 Hydrogenation of CO . . . 19

5 Discussion **21**

6 Conclusion **25**

7 Future outlook **27**

Bibliography **27**

A Appendix 1 **I**
A.1 Temperature ramp I
A.2 Methane oxidation I

1

Introduction

1.1 Background

Frequently released climate reports give increasingly stronger evidence for a significant impact on the environment due to anthropogenic emissions of greenhouse gases [1]. In order to reduce our impact it is necessary to prevent carbon dioxide (CO_2), nitrous oxide (N_2O), methane (CH_4) and chlorofluorocarbon (CFC) from accumulation in the atmosphere. Since a large proportion of the emissions come from combustion of fossil fuels, which has a great economic significance as well as being an essential part of many people's everyday life, it implies that a prohibition is likely distant. To decrease pollution, development of new efficient processes with reduced environmental footprint or, processes that can convert greenhouse gases to suitable chemical compounds is vital. A driving force to accelerate this development may be achieved by introducing high emission taxes world wide. Future depletion of fossil reserves also implies an increased economic gain in the usage of abundant CO_2.

Many independent research articles state that CO_2, which alone is responsible for more than 50% of the total human made climate impact [2], can be converted to CH_4 through the Sabatier reaction described by eq. 1.1 [3]. The less abundant but poisonous greenhouse gas carbon monoxide (CO) can also be converted to CH_4 according to eq. 1.2 [3]. Reactions 1.1 and 1.2 indicate that the complete reaction of one mole of CO_2 or CO, require four and three moles of hydrogen gas (H_2), respectively. For large amounts of CO_2 this means that even larger quantities of H_2 will be consumed. For instance, the volume concentration of CO_2 in flue gas from a coal-fired power plant is approximatelly 15 %, which means that nearly all of the carbon is converted to CO_2, and the remaining part of the flue gas consists almost entirely of nitrogen and water [4]. To keep the hydrogenation reaction environmental friendly, it is thus important to use hydrogen gas from a renewable source. Life cycle assessment suggests that the most sustainable way of producing hydrogen is *via* water electrolysis by wind, solar or hydropower generated electricity [6]. Today, around four percent of the available hydrogen gas comes from water electrolysis, where only a fraction of the energy used in this process comes from renewable sources. Research on sustainable hydrogen gas production is however ongoing, which may lead to reduced costs and increased access in the future [6]. With new good technology, surplus energy from *e.g.* wind power during nights can be used to produce H_2 and thus store energy until high demand is required.

$$CO_2 + 4H_2 \rightarrow CH_4 + 2H_2O \qquad \Delta H = -165kJ/mol \tag{1.1}$$

$$CO + 3H_2 \rightarrow CH_4 + H_2O \qquad \Delta H = -206kJ/mol \tag{1.2}$$

Promising locations for the methane producing process will primarily be large CO_2 emitting industries, such as fossil fuel fired power plants, chemical and petrochemical manufacturing sites, biorefineries and paper mills. Sites like these can likely handle the potentially large amounts of produced methane. Ideally, companys will be able to make a profit by selling CH_4 instead of paying expensive emission taxes. Since in many countries natural gas infrastructure is well-developed, no major investments are needed to store and transport the renewable methane to users [6].

Previously Aziz *et al.* reported interesting results of CO_2 methanation under atmospheric pressure for metal-promoted mesostructured silica nanoparticle (MSN) catalysts [7]. Both nickel and rhodium promoted catalysts show high CO_2 conversion and selectivity towards CH_4 and were therefore selected as active phases here. In the study by Erdöhelyi *et al.* it is shown that methane is the main hydrogenation product for highly dispersed palladium on different supports [8]. The study also revealed that catalysts with poorly dispersed palladium lead to formation of CO at atmospheric pressure and methanol formation at elevated pressure (9.5 atm).

1.2 Aim

The aim of this thesis is to explore catalyst formulations for the reduction of CO_2 and CO at atmospheric pressure and investigate how temperature and reactant ratio influence the catalyst activity and reaction selectivity. To accomplish this, catalysts consisting of either Pd, Ni or Rh supported on the high surface area metal oxides silica, alumina, ceria, MCM-41 and ZSM-5 were prepared, characterized and evaluated using a chemical flow reactor. Based on the kinetic data, catalyst properties and plausible mechanisms are discussed.

2

Theory

2.1 Heterogeneous catalysis

This thesis focus on heterogeneous catalysis, where the reactants originally is in the gas phase but reacts on the surface of a solid catalyst. Such catalysis relies on adsorption which is a phenomenon where molecules from the gaseous phase attach onto the solid surface. The fundamental principles behind adsorption originates from the thermodynamic driving force to decrease surface free energy. Strong adsorption involves molecular bond breakage when the new bonds between the reactants and the solid surface are created. This is called chemisorption in contrast to the weaker form of adsorption without bond breakage called physisorption. Figure 2.1 shows the relationship between the two types of adsorption as a plot of the potential energy against the distance from a surface for two atoms and one molecule. As expected the potential energy for the molecule (A_2) is zero far from the surface as it is unaffected by the attractive Van der Waals forces. Upon approaching the surface, it reaches a minimum due to increased electronic repulsion. In this dwell the molecule is physisorbed on the surface and can diffuse over long distances if the temperature is not too low. If the physisorbed molecule gains enough energy to approch the surface sufficently close it can, depending on internal bond strength, either dissociate into atoms or chemisorb molecularly [9].

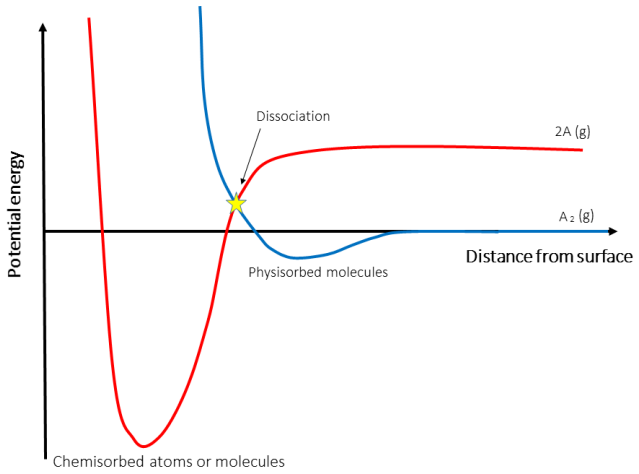


Figure 2.1: Energy path for atoms (red) and molecules (blue) approaching a surface.

The chemical reaction efficiency can be improved by using an appropriate catalyst that lowers the barrier for the reaction (activation energy, E_a). In figure 2.2 the activation energy for a gas phase reaction is compared to that of a catalytic reaction. It is clear that the required energy to pass the barrier is lower when an appropriate catalyst is present. A catalytic reaction follows a catalytic cycle starting with reactant adsorption, followed by a surface diffusion and reaction and finally desorption of products into the gas phase. A simplified explanation of the surface reaction as being more efficient than a gas phase reaction is that the probability of the adsorbed species to collide when diffusing around onto the catalyst surface (two dimensional) is higher compared to gas molecules free to move in three dimensions. The result is formation of new molecules that could be either desired products, unwanted products or intermediates. Creation of intermediates with otherwise unstable configuration is possible by stabilizing surface bonds. The total energy difference between reactants and products are however the same for the two reactions [9].

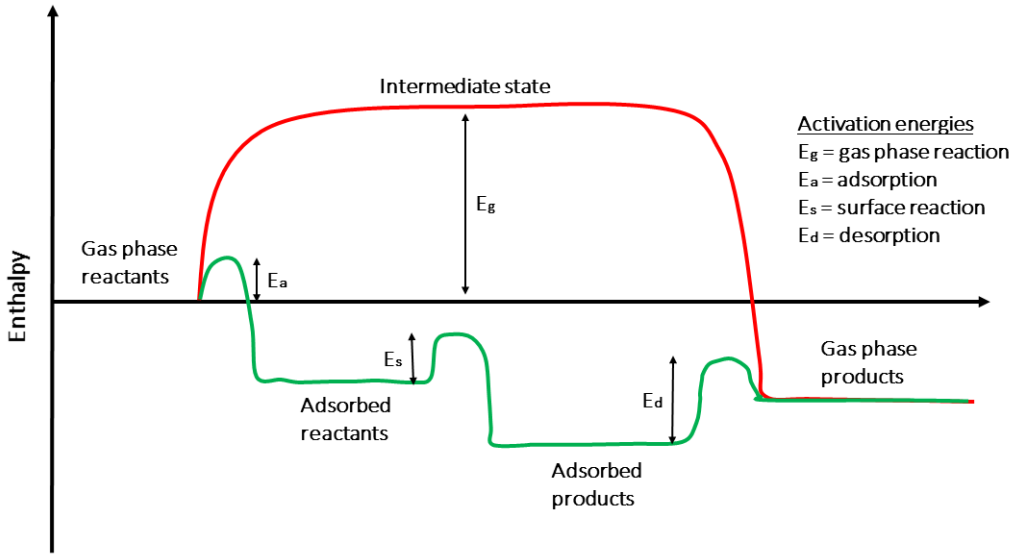


Figure 2.2: Plot of activation energies for an ordinary gas phase reaction (red) and the same reaction with an appropriate catalyst present (green).

A "good" catalyst is recognized by high conversion of involved reactants into desired products (selectivity). Conversion can be calculated by dividing the amount of used reactants by the amount of initial reactants (eq. 2.1). Moreover, one way to calculate selectivity is to use the fraction of a desired product over all products (eq. 2.2).

$$Conversion = \frac{n_i(t=0) - n_i(t)}{n_i(t=0)} \tag{2.1}$$

$$Selectivity = \frac{Desired\ product}{All\ products} \tag{2.2}$$

2.2 Catalyst materials

2.2.1 Common supports

As described above, heterogeneous catalysis is a surface phenomenon and hence a large surface area is usually preferred for catalysts designed to give high conversions. To achieve as large surface area as possible of the usually more expensive active metal, high dispersion of the metal onto a refractory metal oxide known as the support is common. The support should have a high surface area and interact with the metal particle sufficiently strong. Refractory oxides like alumina (Al_2O_3), ceria (CeO_2) and silica (SiO_2) often used as these are able to prevent the small metal particles from agglomeration, and thus prolong the catalyst lifetime [9]. The large specific surface area for these oxides originate from the structure which contains small sized particles connected to each other. In rare cases a large surface area can be unfavorable due to occurrence of continued reactions of desired products, which result in decreased selectivity [9].

Depending on the natre of the support and active metal, electron transfer from the support material can charge a well dispersed active metal particle smaller than 3 nm. An active metal with gained charge can become more reactive such that the catalyst activity is enhanced [9]. Another beneficial feature of well dispersed active metals on a support is increased amount of interfacial atoms in contact with both support and active metal. These atoms have been proven crucial in several reactions [9]. High metal oxide purity is also important since impurities like alkalis and iron can diffuse in the structure and deteriorate the catalytic efficiency by creating metal alloys or blocking active sites [9].

Alumina and ceria are amphoteric oxides which means that the surface composition and charge depends on the surrounding pH. The isoelectric point of alumina and ceria is approximately 9 and 6.75, respectively [10]. During catalyst preparation it is therefore important to consider the isoelectric point to ensure good adsorption of the precursor for the active phase, which often is a metal salt in water solution. The isoelectric point for silica is around pH 1, which is much lower than for alumina and ceria. Silica is therefore known as a non-amphoteric acidic oxide. Despite a low isoelectric point, the surface of silica stays relatively unchanged until pH above 7 [10]. This means that cationic metal complexes and pH above 7 is needed to achieve strong adsorption. Selection of metal precursor for alumina and ceria catalysts is more optional since the surface becomes either positively or negatively charged depending on pH. Depending on circumstances a charged support surface could either promote or reduce reactivity. Mildly acidic alumina or basic ceria are examples of supports that can participate in reactions with CO_2 by letting the acidic gas adsorb onto their active sites [11, 12].

2.2.2 Zeolites and mesoporous materials

Zeolites are crystalline structures consisting of $[SiO_4]^{4-}$ and $[AlO_4]^{5-}$ tetrahedral building blocks sharing 2, 3 or 4 corners. The tetrahedron linkage is also flexible with angles varying from 120^o to 180^o, which increase structure possibilities. This provides a structure with pores and cavities with diameters less than 2 nm and a very large internal surface area that is able to contain 100 times more molecules than amorphous supports [9, 13].

One major difference between the silicon and aluminium tetrahedra building blocks is the net-negative charge of the aluminium tetrahedra. To compensate and keep electrical neutrality, exchangeable cations like H^+ and Na^+ are held close to the negative sites. Cation exchange alters the catalytic character due to increased space in certain channels allowing larger molecules to enter the zeolite. If monovalent ions such as K^+ are exchanged by divalent ions like Ca^+ only half of the amount is needed for charge compensation. Moreover, Ca^+ is smaller than K^+ and tends to favor sites in smaller channels, which contributes to opening of previously closed paths [13].

Zeolites can be divided into different classes depending on Si/Al ratio. Naturally occurring zeolites are aluminum rich with Si/Al ratios close to 1. Thus, a drawback is deactivation due to loss of aluminium if exposed to acid, steam or water. Since stability is important for catalysts and other applications, several synthetic zeolites with higher ratios and diminished cation content have been invented. The structure of the zeolite ZSM-5 consists of medium sized micro channels ordered in three directions. ZSM-5 lacks bigger cavities in the structure but contains locations with more space where reactions more likely take place. Due to a high Si/Al ratio a limited amount of cations are present in the structure, which might be negative for reactivity, but necessary to achieve a longer catalyst lifetime [13].

Mesoporous materials have pores in the range of 2-50 nm [9]. Compared to zeolites, the diffusion is faster and it is more resistant against pore blockage. MCM-41 is the most widely used form of mesostructured silica and it consists of a very ordered SiO_2 hexagonal network [13]. The reseller, Sigma-Aldrich guarantees a pore size of 2.1-2.7 nm, and a surface area of 1000 m^2/g for their MCM-41.

2.2.3 Active phase

An appropriate active phase is the basis to achieve a high performing catalyst for a particular reaction. To increase reactivity, catalysts are often reduced to eliminate elements like oxygen from its surface. Orbital theory reveal information about the number of electrons in the outer valence orbitals [14]. A trend known as the volcano principle originates from elements position in the periodic system. Metals to the left such as in group 6 and 7 have relatively few electrons and many empty orbitals. Strong bonds to adsorbates are therefore easily formed, causing fully covered active sites. Due to difficulties in surface bond breakage, the lifetime of these adsorbed species becomes long, leading to an inferior catalyst. On the other side, metals far to the right have their d-orbitals filled with electrons, and adsorbate-surface bonds be-

comes weak and rare [9]. Ideal active metals for the majority of catalysts are usually elements in between. Gas molecules approaching these surfaces are capable of adsorbing and dissociating because of increased electron density in empty antibonding orbitals. A result of this becomes weaker bonding orbitals and new surface bonds [9].

Surface structure is another important feature that contributes to catalyst efficiency. Depending on number and distance to neighbouring atoms, surface energy varies. The underlying reason for how atoms are arranged is determined by crystal structure and which kind of miller indices that dominate the metal surface [14]. Due to lower surface energy on a surface with densely packed atoms, it is less likely for molecules to adsorb. An explanation to this is better electron transfer from open surface structures to antibonding orbitals of adsorbates [9]. Beside type of crystalline planes, irregularities such as steps and vacancies in the structure decrease coordination number and increase reactivity. However, one should again mention that too high surface energy may be detrimental to the catalytic performance of particular reactions. A very open structure might create strong bonds that inhibit product desorption, leading to self-poisoning [9].

To utilize the active metal more efficient, a high dispersion is beneficial. Dispersion of an active metal on another surface is calculated by dividing the number of surface atoms by the total number of atoms in the dispersed phase (eq. 2.3). A high dispersion utilizes the active material more efficient, which reduce costs. If dispersed metal particles becomes smaller than 3 nm, their metal character starts to disappear due to splitting of the conduction band [9]. Depending on reaction this can affect catalysis both positively and negatively. This reminiscent of how the temperature affect catalyst reactions. At lower temperatures the surface might be covered by one reactant, and at higher temperatures covered by another.

$$Dispersion = \frac{Number\ of\ surface\ atoms}{Total\ number\ of\ atoms} * 100 \tag{2.3}$$

Palladium, nickel and rhodium are close to each other in the periodic table, indicating a similar nature. Nickel is compared to palladium and rhodium, relatively abundant at earth's crust and therefore much cheaper. It belongs to the fourth period and is substantially lighter than palladium and rhodium in the fifth period. The oxidation state of nickel is usually 2^+ due to the electron configuration of ten valence electrons where two of the electrons prefer to fill the 4s shell and the eight remaining configures into the 3d orbitals [14].

2.3 Catalytic hydrogenation

A hydrogenation reaction can be explained as hydrogen addition to another compound. The active metal is crucial for heterogeneous hydrogenation catalysts since it creates sites where hydrogen molecules can chemisorb and dissociate [14]. The active metal should also be compatible with the other reactants involved in the reaction. Surface collisions between adsorbed hydrogen atoms and CO_2 need less

energy than gas phase collisions to carry out the methanation reaction. An established reaction mechanism for this reaction is not determined, but two main routes were recently proposed in a critical review [15]. One of the proposed mechanisms contain an elementary step where adsorbed CO_2 dissociates to adsorbed CO and O. In the other mechanism, CO_2 undergoes direct hydrogenation to methane and lacks a CO intermediate step. Figure 2.3 shows a set of possible events for the CO_2 hydrogenation mechanism that contains a CO intermediate [15]. Initially CO_2 and H_2 chemisorbs and dissociates on the active metal. The adsorbates starts to diffuse onto the surface and collides with each other, creating CH_4 and water that desorbs from the surface.

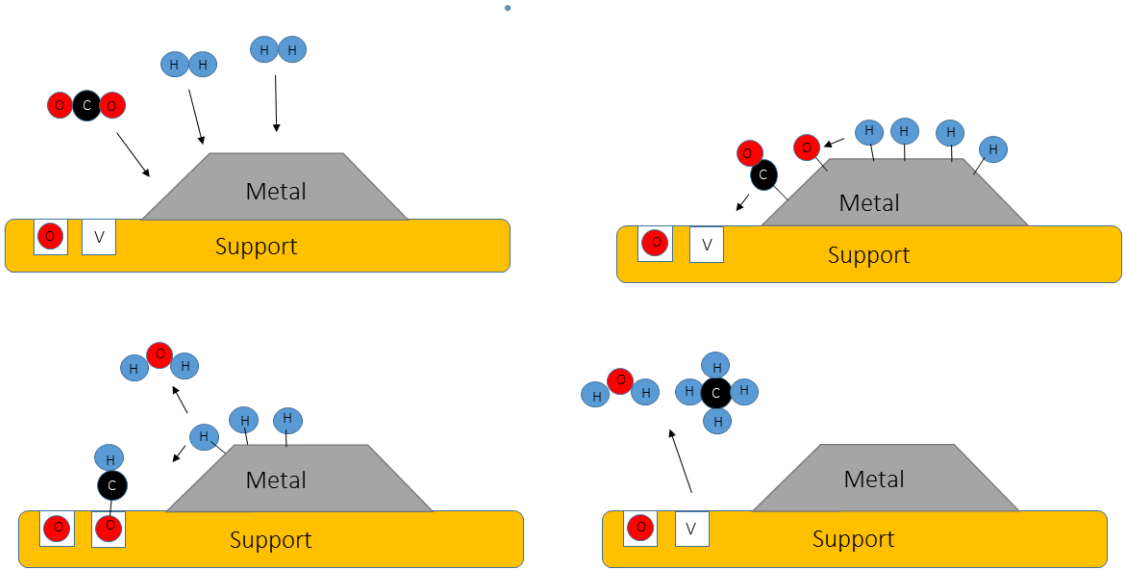


Figure 2.3: Possible methanation mechanism of CO_2

The negative enthalpy for Sabatier reaction, 1.1 tells us that it is an exothermic reaction. Thus, no additional energy is required to carry it out, except of reaction initiation. However, due to the complexity of an eight-electron reduction of the fully oxidized carbon atom in CO_2 a catalyst is crucial to promote the kinetics [15].

3

Experimental section

3.1 Experimental approach

The experimental approach in this thesis consists of three main parts, *viz.* Preparation of catalysts with systematic variation of support material, basic catalyst characterisation of specific surface area and structure and kinetic measurements for each catalyst. Here under, each moment is described in more detail and some background information on used characterization methods is given as well.

3.2 Catalyst preparation

3.2.1 Incipient wetness impregnation

Powders of alumina (Puralox SBa200, Sasol), ceria (99.5 H.S.A. 514, Rhône-Poulenc) and silica (Kromasil Silica KR-300-10, Akzo Nobel Eka Chemicals) were calcined in air at 600 °C for 2 h with a ramping temperature of 5 °C/min to remove carbonaceous impurities and stabilise the structure. Since MCM-41 (Sigma-Aldrich) is more fragile, calcination temperature was decreased to 450 °C for this material. Precursor solutions of 10 wt.% and 7.78 wt.% nickel and rhodium respectively were prepared by dissolving $Ni(NO_3)_2$*$6H_2O$ (Alfa Aesar) and $Rh(NO_3)_3$*$2H_2O$ (Alfa Aesar) salts with MQ-water. To increase solubility of the rhodium salt, 25 droplets of 70% HNO_3 were added. The palladium precursor solution consisted of 12.9 wt.% of the $(NH_3)_4Pd(NO_3)_2$ (Alfa Aesar) complex.

The specific amount of precursor solution to obtain 3 wt.% of the metal was added to 3 g of each support. MQ-water was then added dropwise while slowly stirring until incipient wetness was reached. By freezing the created paste in liquid nitrogen for some minutes with subsequent freeze-drying over night, the water was removed. The alumina, ceria and silica catalyst powders were then calcined at 550 °C in air in a furnace for 1 h, and the MCM-41 catalyst powders were calcined in air at 450 °C for 1 h.

3.2.2 Aqueous ion-exchange

3 g ZSM-5 (SAR 27, Akzo Nobel) was added to a beaker together with 1.5 liter 0.025 molar nickel nitrate solution. After 24 h of stirring at room temperature the solution was filtered and washed with MQ-Water. The aqueous ion-exchanged

zeolite was then dried at 110 °C for 24 h before calcination in air at 450 °C for 1 h with a ramping temperature of 5 °C/min. Table 3.1 gives an overview of all catalysts prepared in this thesis.

Table 3.1: Summary of prepared catalysts.

3 wt.% Pd/Al_2O_3	3 wt.% Ni/Al_2O_3	3 wt.% Rh/Al_2O_3
3 wt.% Pd/CeO_2	3 wt.% Ni/CeO_2	3 wt.% Rh/CeO_2
3 wt.% Pd/SiO_2	3 wt.% Ni/SiO_2	3 wt.% Rh/SiO_2
3 wt.% Pd/MCM-41	3 wt.% Ni/MCM-41	3 wt.% Rh/MCM-41
-	1.5 wt.% Ni-ZSM-5	-

3.2.3 Washcoating

13 monoliths were cut out from a 2 cm thick honeycomb wafer made of coderite, with 400 cpsi (cell per square inch). The received structure had a cylindrical shape with 69 channels. All monoliths were calcined in a furnace at 600 °C for 2 h to remove carbonaceous impurities. 320 mg catalyst powder and 80 mg of the binder material Böhmite (Disperal P2, Sasol) were mixed thoroughly in 4 g MQ-water and 4 g ethanol. The monoliths were dipped into the continuously stirred solution with subsequent drying under hot-gun for 5 minutes. Blocked channels were cleared by a needle before 2 minutes of calcination at approximately 600 °C under hot-gun. The procedure was repeated until the monoliths had gained a weight of 200 mg. The coated monoliths were finally calcined in a furnance at 600 °C for 2 h with a ramping temperature of 5 °C/min.

3.3 Structural characterisation

3.3.1 X-ray powder diffraction

By bombarding copper with electrons, X-rays of different wavelength are created when electrons falls back to vacancies in the innermost shell. These vacancies are generated by electron excitation and the X-ray wavelength depends on from which shell the electron descends back to the innermost shell. For radiation purification a nickel filter is used to obtain uniform K_α radiation with a wavelength of 0.15418 nm. This wavelength is in the same range as the distance between crystalline atoms [13].

A detector is used to collect and measure the X-rays reflected from a finely ground powder, exposed to X-ray from different angles. A long range order of identical unit cells is required to create a distinct diffraction pattern. At specific angles the crystalline powder scatters the X-ray in such a manner that constructive interference gives rise to a diffraction pattern for the sample. The scattering is sperical and each peak corresponds to a single 2θ angle. The peaks contain information about the distance between atomic planes called miller indices (hkl) in the crystall structure.

Broadened peaks are seen for small crystals because there is not enough long range order to produce complete destructive interference between the peaks [13]. By spinning the sample during radiation, the number of scattering crystallites that creates the diffraction pattern increases, which improves the detection signaling noise. The Bragg equation, 3.1 is used to determine the crystal structure of the catalyst and characterise active metals present on the support.

$$\lambda = 2 * d_{hkl} * sin\theta_{hkl} \tag{3.1}$$

d_{hkl} is the distance between crystal planes, λ is the fixed X-ray wavelength and θ_{hkl} is the Bragg angles reflecting atom planes.

Diffraction patterns are typically presented as a plot of intensity *versus* 2θ. The smallest Bragg angle to the left in the plot is caused by the largest d_{hkl} spacing. For a primitive cubic system this means the *100*, *010* and *001* planes since a cubic unit cell has equal sized sides. Decreased distance between the miller indices needs larger angles to obtain constructive interference. The scattering efficiency of an atom is described by the scattering factor, f_0. f_0 increases with the number of electrons that surrounds the atom and decreases for larger Bragg angles [13].

X-ray diffraction comparison of different catalysts with each other and available standardized diffraction pattern provides important information about the sample preparation and metal-support interaction. It is a fast analysis technique that contributes to better understanding of the catalyst.

X-ray diffraction pattern of the catalysts prepared in this study were analysed with a Bruker axs D8 ADVANCE diffractometer with Cu K_α radiation equivalent to 0.15418 nm. The catalyst powder was added to the sample holder where it was flattened with a glass slide until a smooth surface was created. The diffraction data was recorded in the 2θ range of 20–65.88° with incremental steps of 0.028951° for 28 minutes. The sample holder containing the catalyst powder was automatically rotated throughout the whole analysis. The diffraction pattern was then analyzed against reference structures in the software XRD DIFFRAC.EVA.

3.3.2 Specific surface area measurement

Brunauer, Emmett and Teller (BET) once derived a method to measure specific surface area (SSA). Their method is based on knowledge that N_2 physisorption occurs on almost all kind of surfaces at 77 K and low pressure. Initially, a monolayer of adsorbed molecules is assumed to be formed when N_2 gas is added. The instrument device inserts measured parameters in the BET equation 3.2 and extrapolates the slope to the intercept, which contains the monolayer volume (V_m) term. By determination of V_m, the surface area can be calculated according to equation 3.3, where A_m is the area of a nitrogen molecule and N_A/V_A is Avogadro's number per cubic meter. SSA is finally calculated by dividing SA with the weight of the catalyst.

$$\frac{P}{V(P_0 - P_1)} = \frac{1}{V_m * C} + \frac{(C-1)}{V_m * C} * \frac{P}{P_0} \tag{3.2}$$

$$SA = V_m * A_m * \frac{N_A}{V_A} \tag{3.3}$$

The specific surface area was analyzed with a Micromeritics TriStar 3000 instrument. Empty glass tubes were first filled with approximately 200 mg of catalyst powder and dried in nitrogen atmosphere at 230 °C for 3 h. The dry weight of the catalyst powder was measured and reported for each sample to the instrument before the tubes were attached to the Micromeritics TriStar 3000 instrument and drained on gas until vacuum was obtained at cryogenic temperature. Nitrogen gas was then added in small controlled doses and left until equilibrated pressure was formed at each stage. Calculation of adsorbed gas quantity was performed and the procedure was repeated until a monolayer was formed, and then continued until saturation, which indicates that all pores are filled. With all pores filled, the instrument starts draining the tubes on gas again and proceeds until vacuum. BJH (Barett, Joyner, Halenda) calculations could then be used by the instrument to determine the pore volume.

3.4 Kinetic evaluation

The catalytic performance for each catalyst was analyzed in a continuous gas flow reactor. In figure 3.1 a schematic setup for the gas flow reactor is shown. A decided gas composition flows into a quartz tube reactor with a rate of 2000 ml/min. The reactor contains a coated monolith catalyst surrounded by two uncoated monoliths, placed close to the outlet. The catalyst and the monoliths were wrapped in a thin layer of quartz wool to prevent bypassing of gas. One thermocouple was placed in the middle of the catalyst and another one in the middle of the first monolith. Temperature was regulated by voltage changes to a heating coil that surrounds about half of the quartz tube. The whole reactor was covered in a thick layer of quartz wool to reduce heat loss. A FTIR instrument (MKS 2000) was used to analyze the outlet gas. To ensure that the instrument gave reliable measurements, it was calibrated without any catalyst present.

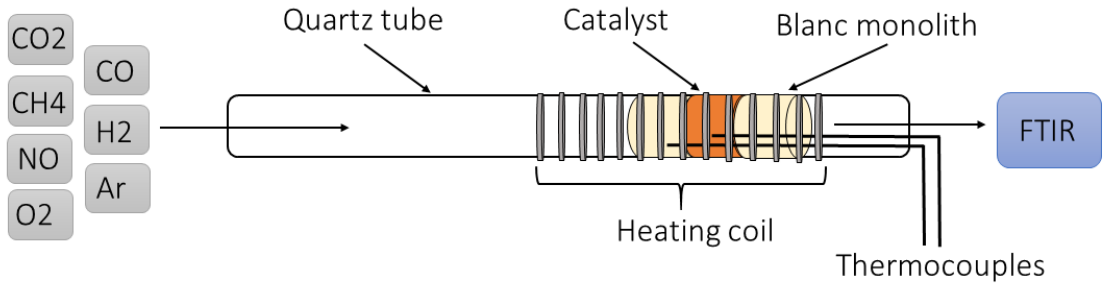


Figure 3.1: Setup for the flow reactor experiments.

Each catalyst was investigated with an almost 9 hours long script, according to table 3.2. The test started with 5 minutes of oxidizing and 5 minutes of reducing pretreatment at 450 °C. A gas mixture of 1% CO_2 and 5% H_2 in argon was then turned on for 10 minutes, corresponding to a 1:5 ratio. At the second step, three different ratios of CO to H_2 were tested. The two last steps were hydrogenation of NO and methane oxidation. Between every step in the script, a 5 minute flush with argon was made to clean the catalyst surface. The same procedure, except for the pretreatment step was repeated at 350, 250 and 150 °C.

Table 3.2: Gas sequence carried out at 150, 250, 350 and 450 °C using a total flow rate of 2000 ml/min. The time at each step was 10 min.

Step	CO_2 (%)	CO (%)	NO (%)	CH_4 (%)	H_2 (%)	O_2 (%)	Ar (%)
1	0	0	0	0	0	5	95
2	0	0	0	0	5	0	95
3	1	0	0	0	5	0	94
4	0	1	0	0	5	0	94
5	0	1	0	0	3	0	96
6	0	1	0	0	1	0	98
7	0	0	0.05	0	0.15	0	99.8
8	0	1	0.05	0	0.15	0	98.8
9	0	0	0	0.1	0	2	97.9
10	0	0	0	0.1	0	0.025	99.875

4

Results

4.1 Characterization of catalysts

Nitrogen adsorption measurements, summarised in table 4.1 reveal that all prepared catalysts have large specific surface areas. Palladium impregnated metal oxides have slightly larger surface areas than nickel impregnated, which in turn are slightly larger than the ones with rhodium. As expected from previous studies where metal oxides from the same fabricators were used [16] [17], silica catalysts had the largest surface area ($\sim$ 315 m^2/g), followed by alumina ($\sim$ 285 m^2/g) and ceria ($\sim$ 130 m^2/g). Measurements on MCM-41 and ZSM-5 were cancelled due to the long measurement times, which indicate that the large surface areas promised by reseller, presumably are retained.

Table 4.1: Nitrogen adsorption measurements of surface area and pore volume for the catalysts with alumina, ceria and silica support.

Catalyst	Specific surface area (m^2/g)	Pore volume (cm^3/g)
Pd/Al_2O_3	186.9	0.50
Ni/Al_2O_3	181.8	0.49
Rh/Al_2O_3	180.2	0.49
Pd/CeO_2	131.1	0.18
Ni/CeO_2	128.2	0.18
Rh/CeO_2	125.2	0.18
Pd/SiO_2	315.3	0.86
Ni/SiO_2	311.1	0.86
Rh/SiO_2	309.5	0.86

The results from XRD analysis of all samples are shown in figure 4.1. It can be seen that the pure metal oxide patterns are unaffected by calcination at 600 °C and impregnation of palladium, nickel and rhodium. The alumina, ceria, silica, MCM-41 and ZSM-5 patterns were all confirmed by a reference database software named XRD DIFFRAC.EVA. The same software was also used to identify the clearly visible peaks that appeared for the impregnated silica and MCM-41 supports. These peaks were found to correspond to the diffraction pattern of palladinite (PdO), bunsenite (NiO) and rhodium oxide (Rh_2O_3), seen as colored rods above the x-axis.

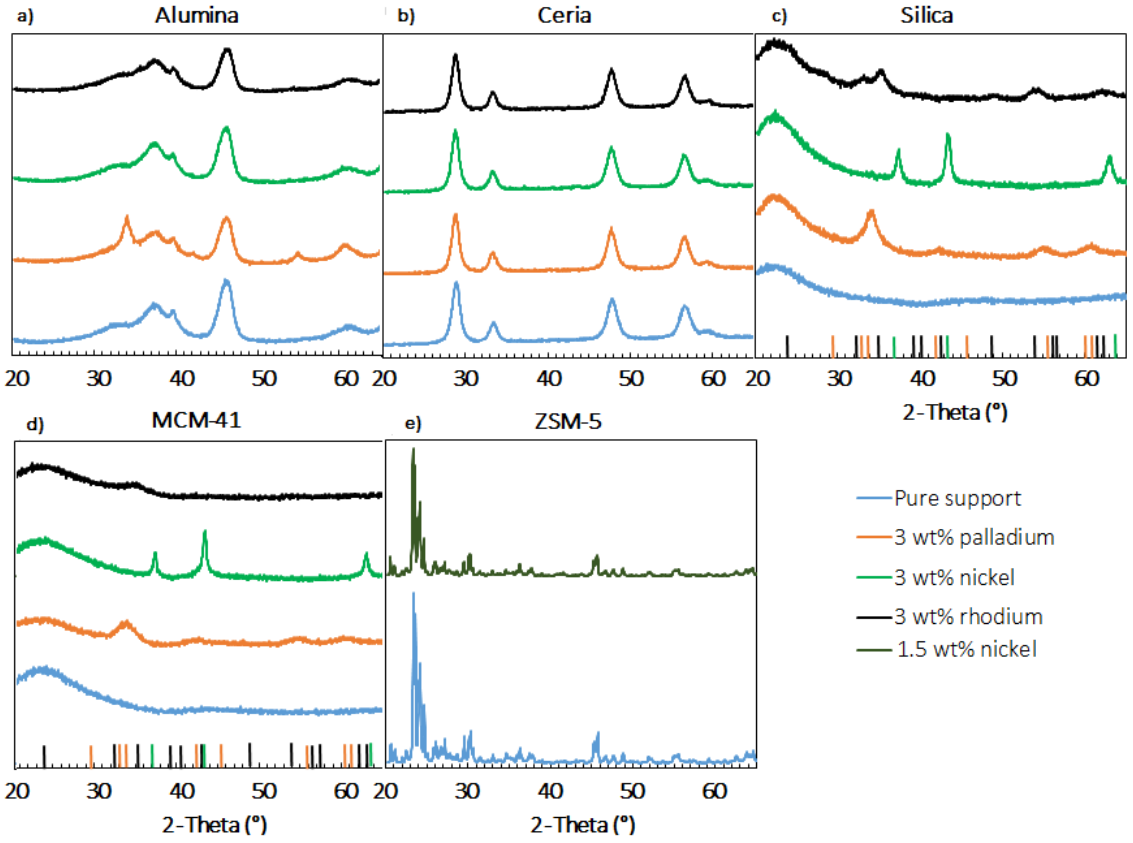


Figure 4.1: XRD pattern of palladium, nickel and rhodium impregnated on a) alumina, b) ceria, c) silica, d) MCM-41 supports. e) shows the the XRD pattern for 1.5 wt.% nickel ion exchanged into ZSM-5.

4.2 Catalysts performance

4.2.1 Hydrogenation of CO_2

Figure 4.2 shows the catalytic performance of metal-promoted alumina, ceria and silica catalysts as steady-state outlet concentrations of CO_2, CH_4 and CO plotted against corresponding temperature. The inlet gas concentrations to the flow reactor are 1% CO_2 and 5% H_2 in argon and each point in the following figures is a calculated average value over a ten-minute period. The temperature dependence of CO_2 hydrogenation can clearly be seen for the three support materials. In the left column for alumina, barely 0.05% CH_4 is formed at 250 °C for the rhodium catalyst, compared to 0.425% at 350 °C. Despite a significant increase in CO_2 conversion from 350 to 450 °C, the formation of CH_4 is slightly decreased. In contrast to this reduction, CO formation increases from 0 to 0.22%. A similar increase in CO concentration from 0 to 0.14% is seen for the Pd/Al_2O_3 catalyst at 450 °C. The remaining part of the converted CO_2 becomes CH_4. The least active alumina catalyst, which shows minor CO_2 reduction at elevated temperature is the nickel containing sample.

For the ceria supported catalysts a major CO_2 reduction is observed (middle column of figure 4.2) at 350 and 450 °C. A significant difference in product selectivity between the active metals is however seen. Unlike the declining CH_4 formation for Rh/Al_2O_3, an increase from 0.44% to 0.47% is observed when temperature is increased from 350 to 450 °C for the Rh/CeO_2 catalyst. Analogous to the alumina catalyst, CO formation increases much more at higher temperatures and becomes the main cause for the increased CO_2 turnover. The Ni/CeO_2 catalyst follows the same trend as Rh/CeO_2 but with lower CH_4 and higher CO formation. For the Pd/CeO_2 catalyst, almost all the converted CO_2 becomes CO at 450 °C in a way that no other catalyst studied resemble.

The silica supported catalysts in the right column shows the overall lowest formation of CH_4. Among the promoting metals, nickel results in highest CO_2 conversion at 450 °C. Around two-thirds of the converted CO_2 in this case becomes CO. A rather more conspicuous selectivity is seen for Rh/SiO_2, where around 80% of the total CO_2 conversion becomes methane. Among the three rhodium catalysts, the one with silica support shows the lowest CO_2 conversion at each temperature.

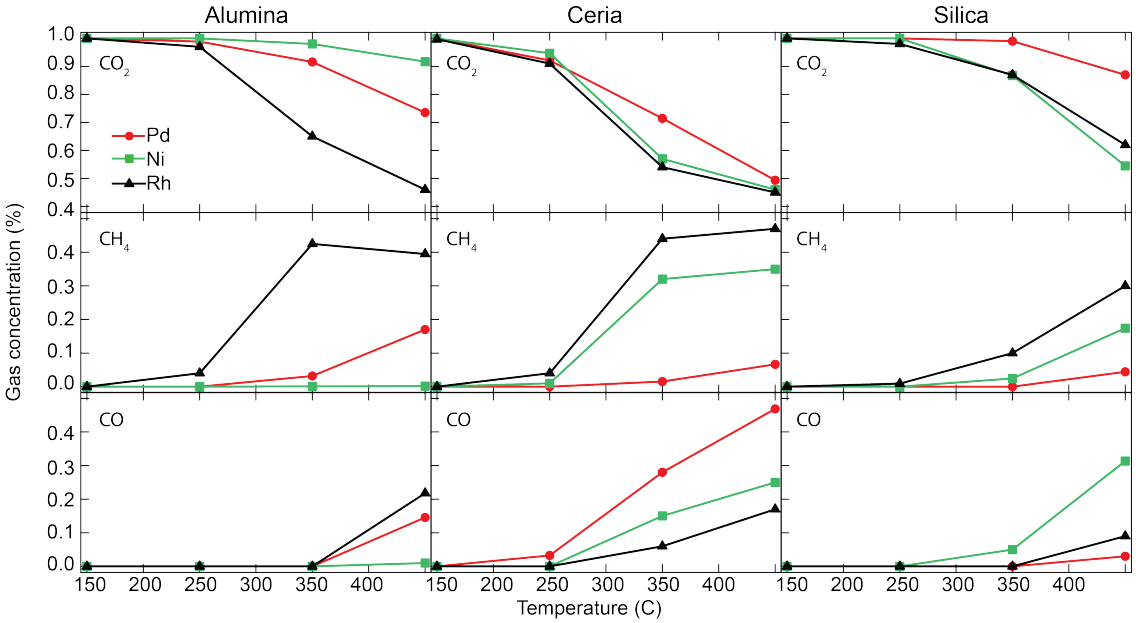


Figure 4.2: Steady state outlet gas concentration of CO_2 (top row), CH_4 (middle row) and CO (bottom row) as a function of temperature during the reaction between 1% CO_2 and 5% H_2 in Ar gas with a total flow rate of 2000 ml/min at atmospheric pressure. Analysed catalysts have alumina, ceria and silica supports, impregnated by palladium, nickel and rhodium.

The catalytic activities of four other catalysts with more complex support materials are summarised in figure 4.3. The result from catalysts with MCM-41 support reminiscent very much of the ones just described for silica, but with a higher CH_4 product selectivity for Rh/MCM-41. According to XRF measurements made by Akzo Nobel, only 1.5 wt.% nickel is exchanged into the ZSM-5 structure. Due to low catalytic activities, the result of MCM-41 and ZSM-5 catalysts will not be

reported any further in this section.

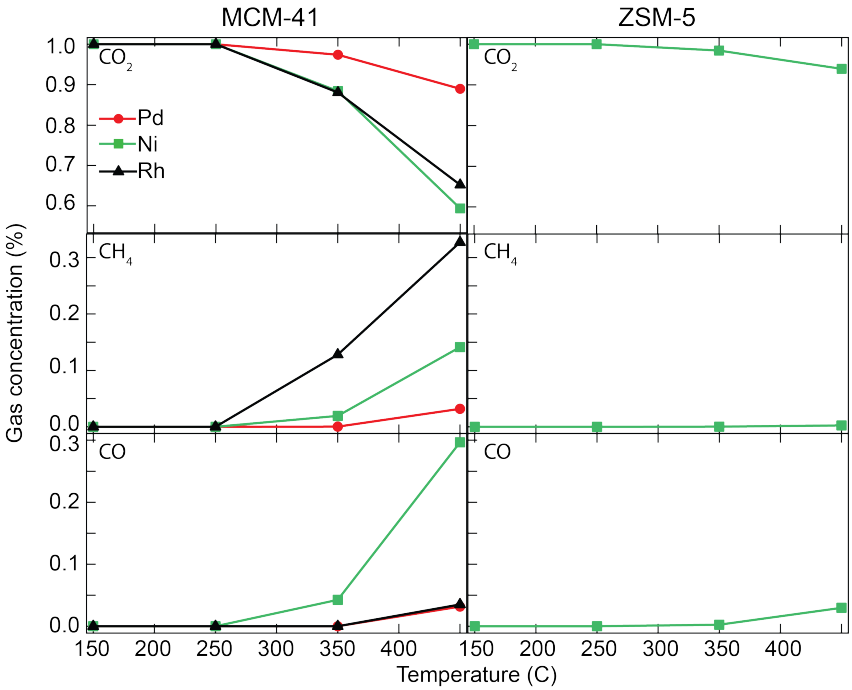


Figure 4.3: Steady state outlet gas concentration of CO_2 (top row), CH_4 (middle row) and CO (bottom row) as a function of temperature during reaction between 1% CO_2 and 5% H_2 in Ar gas with a total flow rate of 2000 ml/min at atmospheric pressure. Analysed catalysts have MCM-41 support impregnated by palladium, nickel and rhodium and ZSM-5 support ion exchanged by 1.5 wt.% nickel.

The results of a deeper investigation of catalytic CO_2 hydrogenation for the Rh/CeO_2 catalyst are shown in figure 4.4. The test is carried out by measuring steady state outlet gas concentrations for inlet concentrations of CO_2 between 0.3% to 1.5% (left column) and H_2 between 1% to 5% (right column) fed to the reactor. Since no reaction was observed at 150 °C during the previous test, the investigation focused on measuring catalytic activity at 250 (blue), 350 (orange) and 450 °C (grey).

At 250 °C, the outlet gas concentration of CO_2 is the same as the inlet concentration in both columns, which means that no reaction occurs. The curves for 350 and 450 °C are similar to each other with the exception that more CO is formed at 450 °C. Above an inlet CO_2 concentration of 1%, the increased CO formation gives rise to a slightly higher CO_2 conversion. Initially, for low inlet concentrations of CO_2, the left column shows a higher CH_4 formation at 350 °C compared to 450 °C. At 350 °C, a maximum value of 0.51% CH_4 is measured for an inlet CO_2 concentration of 0.7%. The formation of CH_4 is then slightly decreased with increased inlet concentration of CO_2 and becomes lower than at 450 °C for an inlet CO_2 concentration of 1.5%.

In the right column one can see a linear increase in CH_4 formation with the same gradient at both 350 and 450 °C when inlet H_2 concentration is increased. At the same time, CO formation decreases linearly with a less steep slope. For an inlet H_2

concentration of 5%, around 0.5% CH_4 is formed. This value corresponds to the one in the left column for an inlet CO_2 concentration of 1%. The remaining gas concentrations of CO_2 and CO at this point are also compatible with each other.

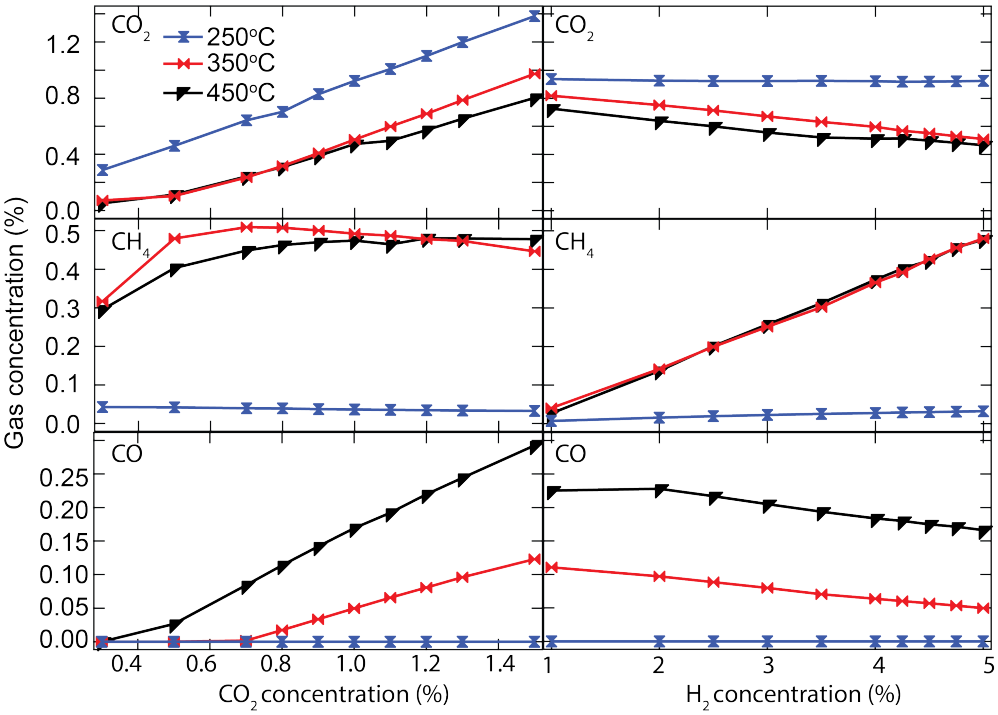


Figure 4.4: Steady state outlet gas concentration of CO_2 (top row), CH_4 (middle row) and CO (bottom row) as a function of inlet concentration of CO_2 with constant H_2 of 5% (left column) and inlet concentration of H_2 with constant CO_2 of 1% (right column), in Ar gas with a total flow rate of 2000 ml/min at atmospheric pressure for Rh/CeO_2.

4.2.2 Hydrogenation of CO

In figure 4.5, hydrogenation of CO is studied for the alumina, ceria and silica supported catalysts. The figure shows a similar trend as hydrogenation of CO_2, but with lower conversions at 350 °C and higher conversions at 450 °C for the majority of the catalysts. The lowest catalytic activity is also here observed for Ni/Al_2O_3 and Pd/SiO_2 with an almost non-existent CO turnover. The best catalyst is once again Rh/CeO_2 that converts 83% of the inlet CO, to almost exclusively CH_4 at 450 °C. Noteworthy is the sharp temperature dependence, observed by the absence of CO conversion at 350 °C for Rh/CeO_2 and Rh/SiO_2. This low turnover is not seen for the rhodium impregnated alumina catalyst where 57% of the CO is converted to CH_4 at 350 °C. Steady state conditions was not achieved at 350 °C for the Ni/CeO_2 catalyst. Unlike all other measurements the outlet CO concentration for the Ni/CeO_2 catalyst increased linearly from 0.15% to 1% throughout the ten-minute period.

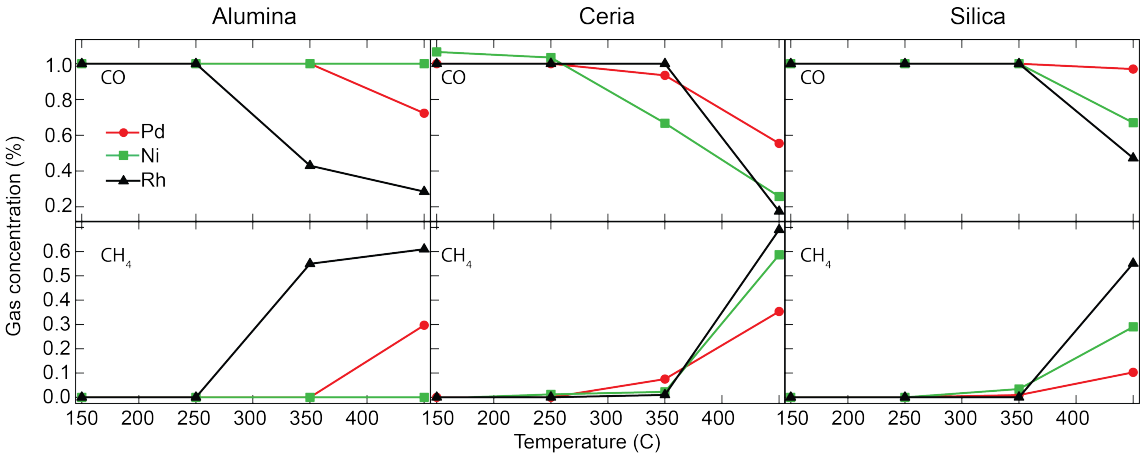


Figure 4.5: Steady state outlet gas concentration of CO (top row) and CH_4 (bottom row) as a function of temperature during the reaction between 1% CO and 5% H_2 in Ar gas with a total flow rate of 2000 ml/min at atmospheric pressure.

Catalytic hydrogenation of CO with Rh/CeO_2 is investigated in a similar manner as hydrogenation of CO_2, and the results are summerised in figure 4.6. Like in figure 4.5, no CO conversion seems to occur at 250 and 350 °C. In the left column, total conversion of CO with high selectivity against CH_4 formation is observed at 450 °C for low inlet concentrations. Outlet concentrations of CO and CH_4 increases slightly for higher inlet concentrations of CO. Formation of CH_4 seems to level out around 0.8%, which is approximately 0.3% higher than for CO_2 hydrogenation. A correlation between measured values in left and right column is however not observed.

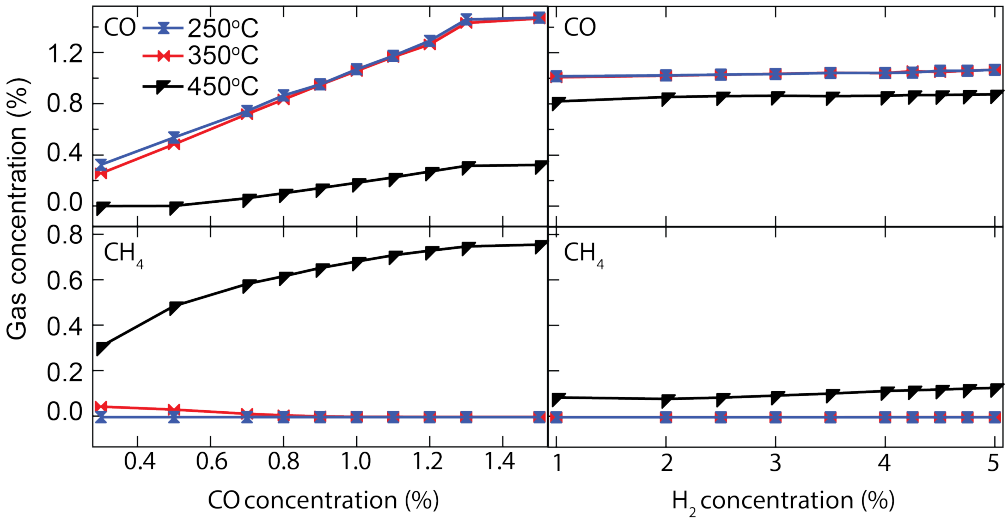


Figure 4.6: Steady state outlet gas concentration of CO (top row) and CH_4 (bottom row) as a function of inlet concentration of CO with constant H_2 of 5% (left column) and inlet concentration of H_2 with constant CO of 1% (right column), in Ar gas with a total flow rate of 2000 ml/min at atmospheric pressure for Rh/CeO_2.

5
Discussion

The aim of this thesis is to explore catalyst formulations for the reduction of CO_2 and CO at atmospheric pressure and investigate how temperature and reactant ratio influence the catalyst activity and reaction selectivity. For this purpose catalysts consisting of either Pd, Ni or Rh supported on silica, alumina, ceria, MCM-41 and ZSM-5 were prepared, characterized and evaluated using a chemical flow reactor. All catalysts were prepared similarly using incipient wetness impregnation with ZSM-5 being the only exception where instead aqueous ion-exchange was employed. The results from the specific surface area (BET analysis) measurements and XRD analysis reveals that metal impregnation of support materials and subsequent freeze-drying and calcination were accomplished with preserved structure of the support. Furthermore, the total absence of peaks for metal phases in the diffractograms, besides the ones for ceria indicates a successful impregnation, resulting in highly dispersed metal particles with diameters smaller than the XRD detection limit of about 3 nm. Similar results have been confirmed by STEM in an earlier study [18]. Another explanation, although less likely, of the absence of metal related peaks may be that the amount of detectable metal particles is too low to cause a measurable diffraction pattern. However, judging by the kinetic measurements the samples show considerable activity (generally) and the observed trends indicate reliable flow-reactor measurements. The forthcoming discussion is therefore focused on the kinetic measurements with some reflections on responsible catalytic properties and plausible mechanisms.

A general trend seen through all of the flow-reactor experiments is an increased conversion at higher temperatures. An inlet CO_2 concentration of 1% is for example indicated in figure 4.3 by the measured outlet gas concentration at 150 °C for the nine catalysts, since no reaction takes place at this temperature. The main reaction products formed during CO_2 hydrogenation at 250, 350 and 450 °C are CH_4, CO and water. A clear trend is promoted formation of CO at increased temperature, due to occurrence of the reversed water gas shift reaction 5.1 [19]. The idea of continued promotion of CO formation above 450 °C is strengthened by a temperature ramped experiment for the Rh/CeO_2 catalyst, seen in figure A.1. This figure also shows that CH_4 formation peaks at a specific temperature around 380 °C and then declines. The linear relationship between increased inlet concentration of H_2 and CH_4 formation observed in the right column of figure 4.4 explains the maximum formation value around 0.5% CH_4 for an inlet H_2 concentration of 5%. To obtain higher CO_2 conversion and CH_4 formation than this, it is therefore necessary to increase the H_2:CO_2 ratio. One indication that this suggestion applies is seen for low inlet CO_2 concentrations at 350 °C for the Rh/CeO_2 catalyst. In the case of

CO_2 concentrations under 0.5% fed to the reactor together with 5% H_2, total CO_2 conversion against CH_4 formation is achieved.

$$CO_2 + H_2 \rightarrow CO + H_2O \qquad \Delta H = 41.2kJ/mol \tag{5.1}$$

Comparison of the active phases used in this thesis clearly shows how much catalytic activity differs between neighboring metals in the periodic table. Rhodium catalysts are more prone to form CH_4 compared to catalysts with palladium and nickel, where larger concentrations of CO is formed. Catalysts with palladium shows the lowest hydrogenation activity, but are by far the best when it comes to methane oxidation in lean conditions. Nickel promoted catalysts tend to be in between rhodium and palladium when it comes to CH_4 selectivity, except for the catalyst with alumina support that lacked catalytic ability. It should be mentioned that 3 wt.% active phase is used instead of 3 mol%. This means that more nickel atoms are used, which may hamper the comparison. To make a fair active phase comparison, particle size and dispersion should be the same. However, the results indicate that a catalyst with rhodium support should be used if as high CH_4 formation as possible is desired. To reduce costs, but still retaining high catalytic ability, half of the rhodium mass may be exchanged by nickel. Palladium catalysts may more likely be used in other purposes, but production of syngas, which mainly consists of H_2 and CO may be an interesting idea to evaluate.

As mentioned in the end of section 2.2.1, both mildly acidic supports like alumina and basic supports like ceria may interact with CO_2, which can contribute to increased activity. Usage of appropriate metal precursors and pH during catalyst preparation is another important aspect to keep in mind when support materials are compared. By focusing on the trends in figure 4.2 and 4.3, one can see that ceria supported catalysts are most active. It is difficult to determine whether this depends on superior interaction between ceria and CO_2, highest active metal dispersion on this support or a combination of both. One thing that is certain is that ceria has smaller surface area compared to alumina, silica and MCM-41, making this a less important parameter. A more important aspect is probably surface area of the active phase, which according to XRD analysis probably is large on ceria and alumina catalysts. When it comes to support-CO_2 interaction, a more specific *in situ* analysis of the catalyst surface is needed to say for sure that ceria sites are more prone to participate in the hydrogenation reaction. However, CO_2 is by nature an acidic gas, and attraction toward the basic cites of ceria may therefore be stronger compared to alumina and silica [12]. Moreover, cerium has the ability to occur in different oxidation states [14], which means that oxygen vacancies on ceria surfaces are not unusual. These oxygen vacancies could also be good places for CO_2 absorption.

In a recently published article by Upham *et al.* it is reported that CH_4 formation by

CO_2 hydrogenation on ruthenium impregnated ceria is sensitive and loses activity when the surface becomes too reduced or oxidized. Opposed to methanation mechanisms in several previously published articles, Upham *et al.* writes that CH_4 is not formed through intermediates of CO or a formate. Infrared measurements instead corresponds to a variety of surface carbonate spectra's [20]. This strengthened the idea of direct CO_2 adsorption and formation of carbonates on ceria supported catalyst, without adsorption and dissociation on the active phase. Most likely, CO_2 also adsorbs on the active phase to some extent and diffuses to the support according to the mechanism in section 2.3. The main advantages of higher metal dispersion seems nevertheless to be a larger surface area for hydrogen to adsorb on, and also increased proportion of metal-support interfaces where the adsorbates can react with each other.

Catalytic activity comparison between silica and MCM-41 that both consists of a network built on silicon and oxygen atoms show almost identical results, despite a nearly three times larger surface area for MCM-41. Beside ZSM-5, these catalysts were the poorest in CO and CO_2 conversion, probably due to low active metal dispersion and no support-reactant interaction. The importance of an active support is obvious for the palladium catalysts that barely shows any catalytic activity for neither silica nor MCM-41 but reaches 50 % CO_2 conversion for the ceria catalyst.

The difference in chemical composition between CO and CO_2 clearly affects the hydrogenation reaction. An indication of this is that CO requires a reaction temperature of 450 °C to react with H_2 and form CH_4 for all catalyst, except Rh/Al_2O_2 where almost 60% is converted at 350 °C. The absent turnover at 350 °C and high CO conversion at 450 °C for Rh/CeO_2 was later confirmed in a new catalytic experiment for different inlet concentrations of CO. An explanation to this phenomena may be that CO desorbs much slower than it adsorbs at low temperatures, compared to CO_2 that has a higher desorption rate, which enable hydrogen to adsorb as well. It is probably the slow desorption rate that leads to a deactivated catalyst with a fully covered active phase of CO at 350 °C. This reasoning can be linked back to the increased CO formation during CO_2 hydrogenation at elevated temperatures, previously referred to as the reversed water gas shift reaction. Figure A.1 shows how CO formation exponentially increases with temperature, which suggests that CO does not spend enough time on the surface to react with hydrogen before it desorbs. An increased desorption rate may therefore decrease the concentration of fully reduced CO_2. Another explanation to this exponential increase may be an increased hydrogen desorption rate, resulting in a lower amount of hydrogen adsorbates for CO to react with on the catalyst. However, the increased CO formation depends most likely as we first proposed to increased desorption rate of CO since a 80% CO conversion is seen for the Rh/CeO_2 catalyst at 450 °C, which is virtually impossible for a high hydrogen desorption rate that results in hydrogen adsorbate absence.

In a similar experiment, different inlet concentrations from 1 to 5% H_2 were fed to the flow reactor together with 1% CO. Surprisingly, only a very low CO turnover was seen at 450 °C this time. An explanation to this result may be that the catalyst

surface rather becomes self-poisoned due to insufficient H_2 adsorption for the hydrogenation reaction to occur. Since the result has not been confirmed in a repeated experiment, it can not be excluded that a measurement error has occurred.

As a reference reaction, oxidation of methane in oxygen excess was carried out for all catalysts. Figure A.2 shows that type of support material is not as crucial for catalytic methane oxidation as we previously stated for the hydrogenation reaction. Choice of active phase is instead totally decisive, and methane is almost fully oxidized to CO_2 for all palladium catalysts at both 350 and 450 °C. Rhodium catalysts does not show as high catalytic activity as palladium at 350 °C, but approaches total conversion at 450 °C. Finally, it seems like nickel catalysts totally lacks any catalytic ability for this reaction, *i.e.* nickel lacks active sites for the reactants to adsorb and dissociate on. These results should be considered, since it is important to know what happens if oxygen is present in the system.

6
Conclusion

This thesis shows that a high CO_2 conversion with 100% selectivity against CH_4, which advantageously can be used as a fuel, is possible to achieve with an appropriate catalyst at 350 °C and optimized reactant ratios. To reach this conclusion, catalysts consisting of either Pd, Ni or Rh supported on silica, alumina, ceria, MCM-41 and ZSM-5 were prepared, characterized and evaluated at different temperatures and molar ratios using a chemical flow reactor. Specific surface area (BET analysis) measurements and XRD analysis indicate a successful catalyst preparation and kinetic measurement data seems reliable.

The most prominent results in this study is observed for the rhodium impregnated ceria catalyst that managed to convert 44% of the CO_2 to almost exclusively CH_4 at 350 °C. An even higher CO_2 conversion is observed at 450 °C, but due to CO formation through the reversed water gas shift reaction, CH_4 selectivity decreases. Further evaluation of Rh/CeO_2 revealed evidence of a maximum CH_4 formation around 380 °C. A linear relationship between increased CH_4 formation and H_2:CO_2 ratio was also observed at both 350 and 450 °C. Gas mixtures of inlet CO_2 concentrations below 0.5% fed to the reactor together with 5% H_2 confirms that a high H_2:CO_2 ratio leads to total conversion against CH_4 formation.

The results, strengthened by previously published material indicate that a metal oxide support like ceria can interact with CO_2 and thus, be a part of and promote the hydrogenation reaction by direct formation of surface carbonates. The importance of an interacting support is obvious for catalysts with a less active phase, like palladium. The catalytic activity for the silica supported palladium catalyst at 450 °C is more reminiscent of the low conversion at 250 °C for the one with ceria support, and only a fraction of the turnover at 450 °C.

Comparison of the catalytic ability of CO_2 and CO hydrogenation shows a clear trend that CO require higher reaction temperatures. An explanation of this behavior is suggested to depend on too low desorption rate of CO below 450 °C, leading to self-poisoning of the active phase and no H_2 adsorption.

7
Future outlook

Suggestions for future work, based on ideas emerged during this thesis, which due to time restrictions could not be evaluated are listed below:

- Perform *In situ* DRIFT spectroscopy experiments to distinguish adsorbed species on alumina, ceria and silica from each other. This can reveal valuable information of how CO_2 interacts with the support, and thereby increase understanding of its role during hydrogenation.
- Prepare catalysts with other techniques such as the sol-gel method, and use a wide range of active phase wt.% to see whether this affects the catalytic activity.
- Evaluate the catalysts more accurate around 380 °C at elevated pressure.
- Do deactivation tests and investigate how common flue gases such as oxygen and sulphur dioxide affects the catalyst performance.
- Is it possible to improve the chemical economy, *i.e.* remove water formation from the Sabatiers reaction and thus, decrease H_2 consumption?

Bibliography

[1] Vancouversystem Tidskriftsartikel Författarens efternamn förnamnsinitial/er. Artikelns titel. Tidskriftens titel. Publiceringsår månad;volym(nummer):sidor. IPCC. CLIMATE CHANGE 2014 Synthesis Report. IPCC. Report number: 5, 2014

[2] http://www.naturvardsverket.se/Sa-mar-miljon/Klimat-och-luft/Klimat/Darfor-blir-det-varmare/Andra-vaxthusgaser/

[3] Xiong J, Dong X, Song Y, Dong Y. A high performance RueZrO2/carbon nanotubeseNi foam composite catalyst for selective CO methanation. Power Sources. 2013 May;242:132-136 catalyst for selective CO methanation

[4] Singh D, Croiset E, Douglas PL, Douglas MA. Techno-economic study of CO2 capture from an existing coal-fired power plant: MEA scrubbing vs. O2/CO2 recycle combustion. Energy Conversion and Management. 2003 Nov;44:3073–3091

[5] EPA (2014). eGRID 2010 data. U.S. Environmental Protection Agency, Washington, DC.

[6] Bhandari R, Trudewind CA, Zapp P. Life cycle assessment of hydrogen production via electrolysis - a review. Cleaner Production. 2014 Dec;85:151-163

[7] Aziz MAA, Jalil AA, Triwahyono S, Sidik SM. Methanation of carbon dioxide on metal-promoted mesostructured silica nanoparticles. Applied Catalysis A: General. 2014 Aug;486:115-122

[8] Erdöhelye A, Pásztor M, Solymosi F. Catalytic Hydrogenation of CO2 over Supported Palladium. Journal of Catalysis. 1986 98:166-177

[9] Bowker M. The Basis and Application of Heterogeneous Catalysis. OXFORD UNIVERSITY PRESS; 1998.

[10] Brunelle JP. PREPARATION OF CATALYSTS BY METALLIC COMPLEX ADSORPTION ON MINERAL OXIDES. Pure Applied Chemistry. 1978;50:1211-1229

[11] Ferreira-Aparicio P, Guerrero-Ruiz A and Rodriguez- Ramos I. Comparative study at low and medium reaction temperatures of syngas production by methane reforming with carbon dioxide over silica and alumina supported catalysts Appl. Catal., A, 1998 May;170:177–187

[12] Djinovic P, Batista J and Pintar A. Influence of active metal loading and oxygen mobility on coke-free dry reforming of Ni–Co bimetallic catalysts. Int. J. Hydrogen Energy, 2012 Jun;37:2699–2707.

[13] Smart L, Moore E. Solid state chemistry: an introduction. 4. ed. Boca Raton: CRC Press; 2012.

[14] Atkins P, Overton T, Rourke J, Weller M, Armstrong F. Inorganic Chemistry 5. ed. OXFORD UNIVERSITY PRESS; 2010.

[15] Wang W, Wang S, Ma X, Gong J. Recent advances in catalytic hydrogenation of carbon dioxide. Chemical Society Reviews. 2011 Jul;40:(7):3703–3727.

[16] Adams EM, Skoglund M, Folic M, Bendixen, Gabrielsson P, Carlsson PA. Ammonia formation over supported platinum and palladium catalysts. Applied Catalysis B: Environmental 2014 Oct;165:10-19

[17] Fouladvand S, Schernich S, Libuda J, Grönbeck H, Pingel T,Olsson E, Skoglundh M, Carlsson PA. Methane Oxidation Over Pd Supported on Ceria–Alumina Under Rich/Lean Cycling Conditions. TOPICS IN CATALYSIS. 2013 Feb;56:410–415

[18] Bounechada D, Fouladvand S, Kylhammar L, Pingel T, Olsson E, Skoglundh M, Gustafson J, Michiel MD, Newtonf MA, Carlsson PA. Mechanisms behind sulfur promoted oxidation of methane. Phys. Chem. Chem. Phys. 2013 Feb;15:8648–8661

[19] Pakhare D, Spivey J. A review of dry (CO2) reforming of methane over noble metal catalysts. Chemical Society Reviews. 2014 Feb;43:7813-7837

[20] Upham DC, Derk AR, Sharma S, Metiu H, McFarland EW. CO2 methanation by Ru-doped ceria: the role of the oxidation state of the surface. CATALYSIS SCIENCE TECHNOLOGY. 2015 Mar;5:1783-1791

A

Appendix 1

A.1 Temperature ramp

Figure A.1 shows the temperature dependence of catalytic hydrogenation for the reaction between 1% CO_2 and 5% H_2. The test starts at 350 ^oC and temperature is increased by 5 ^oC/min to 500 ^oC where it is kept constant for 10 minutes. During this temperature elevation, CH_4 formation initially increases to a maximum value of 0.57% at 380 ^oC before it starts to decline as a result of the reversed water gas shift reaction. CO_2 conversion is however increased and at 500 ^oC the concentration of CH_4 and CO equals each other. A temperature reduction to 150 ^oC passes the same maximum value but ends on zero conversion.

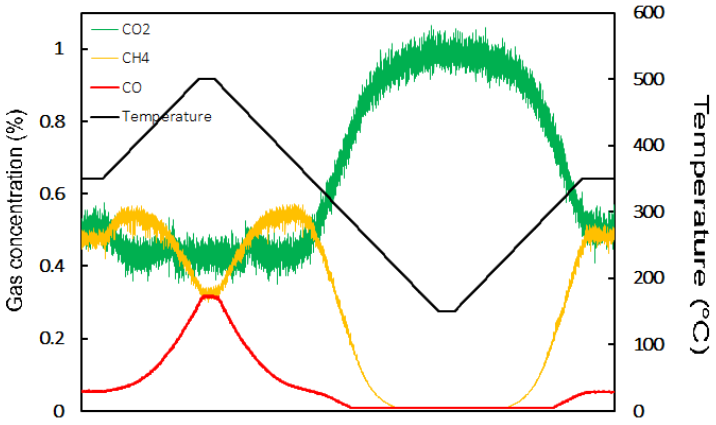


Figure A.1: Outlet gas concentration of CO_2, CH_4 and CO for temperatures between 150 and 500 ^oC during the reaction between 1% CO_2 and 5% H_2 in Ar gas with a total flow rate of 2000 ml/min at atmospheric pressure.

A.2 Methane oxidation

Methane oxidation measurements in lean conditions with oxygen excess are shown in figure A.2 for alumina, ceria and silica catalysts. Catalysts with supports impregnated by palladium shows the highest catalytic activity. Total methane combustion to CO_2 is both seen for Pd/Al_2O_3 and Pd/CeO_2 at 350 and 450 °C. For rhodium catalysts, total methane combustion only occurs at 450 °C when alumina is used as

support material. The figure also reveal that catalysts with nickel as active phase lacks catalytic activity for this reaction.

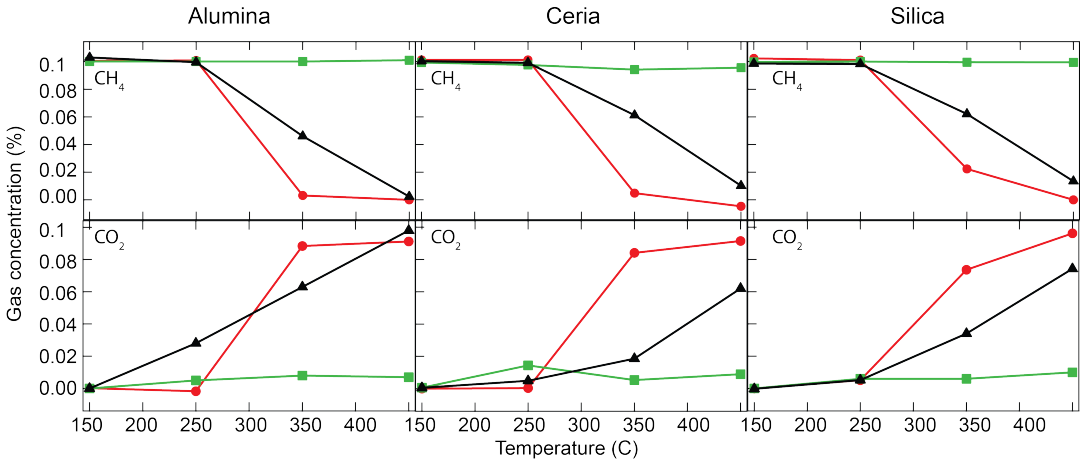


Figure A.2: Steady state outlet gas concentration of CH_4 (top row) and CO_2 (bottom row) as a function of temperature during the reaction between 0.1% CH_4 and 2% O_2 in Ar gas with a total flow rate of 2000 ml/min at atmospheric pressure.